International Journal of Chemical, Materials and Biomolecular Sciences
ISSN: 2415-6620
Vol:5, No:1, 2011

Modeling of Catalyst Deactivation in Catalytic Wet Air Oxidation of Phenol in Fixed Bed Three-Phase Reactor

Akram Golestani, Mohammad Kazemeini, Farhad Khorasheh and Moslem Fattahi

***Abstract*—**Modeling and simulation of fixed bed three-phase catalytic reactors are considered for wet air catalytic oxidation of phenol to perform a comparative numerical analysis between trickle-bed and packed-bubble column reactors. The modeling involves material balances both for the catalyst particle as well as for different fluid phases. Catalyst deactivation is also considered in a transient reactor model to investigate the effects of various parameters including reactor temperature on catalyst deactivation. The simulation results indicated that packed-bubble columns were slightly superior in performance than trickle beds. It was also found that reaction temperature was the most effective parameter in catalyst deactivation.

***Keywords*—**Catalyst deactivation, Catalytic wet air oxidation, Trickle-bed, Wastewater.

I. Introduction

In many industries including petroleum, petrochemical, and pharmaceutical industries, wastewater streams containing organic compounds are generated that are hazardous and toxic to the environment. Phenol is the one of the most important organic pollutant. The importance of phenol in water pollution is due to its high toxicity to the aquatic life and its resistance to biodegradation. Phenol introduces a strong odor and taste to water even at very small concentrations. For wastewater streams having phenol concentration in excess of 130 mg/l, direct biological treatment is not feasible and it is necessary to employ less conventional techniques including chemical oxidation or wet air oxidation.

Wet air oxidation processes (WAO) have a great potential in advanced wastewater treatment facilities [1,2]. Compared with WAO, catalytic wet air oxidation (CWAO) has lower energy requirements and due to presence of a catalyst, higher oxidation rates can be achieved [3]. Consequently, less severe reaction conditions can be employed to reduce the chemical oxygen demand to the same extent in CWAO compared with the non-catalytic process [4,5]. Furthermore, in catalytic wet air oxidation, the catalyst can be regenerated and reused. CWAO is also very flexible and it can be used for treatment of wastewaters containing a wide range of organic and/or inorganic pollutants including carbon (C), oxygen (O), nitrogen (N), halogen (X), sulfur (S), and phosphorus (P)-bearing molecules.

CWAO liquid-phase oxidation processes fall into the category of catalytic gas-liquid-solid reactions that require rather complex mathematical modeling to describe such effects as inter-phase and intra-particle heat and mass transport, reaction kinetics on the porous catalysts, thermodynamics, flow patterns, and hydrodynamics [6]. Relatively few studies have been published dealing with CWAO of organic compounds in large-scale trickle-bed reactors and packed-bubble columns [7,8]. The present study deals with the modeling and simulation of catalytic wet air oxidation of phenol in trickle-bed and packed-bubble column reactors using a 7:3 MnO_2:CeO_2 composite oxide catalyst. Effects of particle diameter, superficial liquid velocity, liquid-solid mass transfer coefficient, external wetting efficiency, inlet phenol concentration, and temperature has been investigated on phenol conversion and catalyst deactivation.

II. Modeling of Catalytic Wet Air Oxidation of Phenol

To analyze the performance of two common three-phase reactors for catalytic wet air oxidation of aqueous solutions containing phenol under deactivating conditions, time and space dependent models were developed employing the following general assumptions for co-current down-flow trickle-bed and co-current up flow packed-bubble column reactors [9]:

1. Phenol is non-volatile and the reaction takes place in the liquid phase.
2. Phenol concentration in the feed is low and reactors are isothermal.
3. The reaction is carried in a large excess of oxygen and equilibrium concentration was assumed for dissolved oxygen.
4. Mass transfer was considered between the dynamic and static liquid holdups and intra-particle liquid.

A. Golestani is with the Department of Chemical and Petroleum Engineering, Sharif University of Technology, Azadi Avenue, P.O. Box 11365-9465, Tehran, Iran (e-mail: Golestani@che.sharif.edu).

M. Kazemeini is with the Department of Chemical and Petroleum Engineering, Sharif University of Technology, Azadi Avenue, P.O. Box 11365-9465, Tehran, Iran (corresponding author to provide phone: +98-21-6616-5425; fax: +98-21-6602-2853; e-mail: kazemeini@sharif.edu).

F. Khorasheh is with the Department of Chemical and Petroleum Engineering, Sharif University of Technology, Azadi Avenue, P.O. Box 11365-9465, Tehran, Iran (e-mail: khorashe@sharif.edu).

M. Fattahi is with the Department of Chemical and Petroleum Engineering, Sharif University of Technology, Azadi Avenue, P.O. Box 11365-9465, Tehran, Iran (e-mail: moslemfattahi@che.sharif.edu)

5. Effective diffusivity in the catalyst was assumed constant and independent of the degree of catalyst deactivation.
6. Diffusion of reactants occurs inside liquid–filled pores.
7. For co-current down-flow trickle-bed reactors both partial and full external wetting may occur while for co-current up-flow packed-bubble columns, only full external wetting is assumed.

The above assumptions set the framework for the mathematical model employed in the current investigation as well as that proposed by Larachi et al. [9].

A. Reaction Mechanism and Kinetics

The reaction between phenol and dissolved oxygen in the liquid phase proceeds on the catalysts surface and deactivation is caused by deposition of carbonaceous species on the active sites. Detailed kinetic investigations using a 7:3 MnO_2:CeO_2 composite oxide catalyst point to a reaction network consisting of the main reaction as well as a number of side reactions involving intermediate and side products [10,11]. The complete reaction-deactivation network describing phenol CWO is shown in Figure 1.

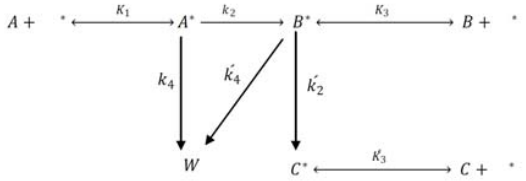

Fig. 1 Reaction-deactivation network for phenol CWO

Accordingly, there are four different lumps involved in the mechanism. Lump A is phenol that can be chemisorbed on the catalyst surface and subsequently converted to chemisorbed aqueous break-down oxidation intermediates, lump B, which in turn further degrades into oxidation end-products, lump C (total inorganic carbon). A series of complex polymerization reactions between lumps A and B, leads to the formation of carbonaceous foulant, lump W, that is irreversibly adsorbed leading to catalyst deactivation by progressive blockage of the active sites on the catalyst surface [12]. The rate of disappearance of phenol and deactivation of catalyst is given by a Langmuir-Hinshelwood-Hougen-Watson type rate expression [10]:

$$-r_A = \frac{k_2 K_1 \alpha C_{Al}}{1 + K_1 C_{Al} + K_3 C_{Bl} + K_3^{'} C_{Cl}} \tag{1}$$

$$r_B = \frac{(k_2 K_1 C_{Al} - k_2^{'} K_3 C_{Bl})\alpha}{1 + K_1 C_{Al} + K_3 C_{Bl} + K_3^{'} C_{Cl}} \tag{2}$$

$$-\frac{d\alpha}{dt} = \frac{(k_4 K_1 C_{Al} + k_4^{'} K_3 C_{Bl})\alpha}{1 + K_1 C_{Al} + K_3 C_{Bl} + K_3^{'} C_{Cl}} \tag{3}$$

B. Reaction and Diffusion within Catalyst Pellets

The transient material balance for diffusion and reaction of species j (representing lump A or B) within the spherical catalyst pellets is given by:

$$\varepsilon_p \frac{\partial C_{jl}}{\partial t} = r^{-2} \frac{\partial}{\partial r}\left(r^2 D_j^{\,eff} \frac{\partial C_{jl}}{\partial r} \right) - \rho_s r_j (C_{Al}, C_{Bl}, C_{Cl}, \alpha) \tag{4}$$

Where the local catalyst activity inside the catalyst pellet can be evaluated by:

$$-\frac{\partial \alpha}{\partial t} = \frac{(k_4 K_1 C_{Al} + k_4^{'} K_3 C_{Bl})\alpha}{1 + K_1 C_{Al} + K_3 C_{Bl} + K_3^{'} C_{Cl}} \tag{5}$$

The initial and boundary conditions for the above equations are as follows:

$$r = 0 \rightarrow \frac{\partial C_{jl}}{\partial r} = 0 \tag{6}$$

$$r = r_p \rightarrow -D_j^{\,eff} \frac{\partial C_{jl}}{\partial r}\bigg|_{r=r_p} = k_{jls}^{d} \eta_e \varphi \left(C_{jl}^{d} - C_{jl}^{*}\right) + k_{jls}^{s} \eta_e (1-\varphi)\left(C_{jl}^{s} - C_{jl}^{*}\right) \tag{7}$$

$$t = o \rightarrow C_{jl}(r,0) = C_{jl}^{0}; \alpha = 1 \tag{8}$$

C. Fixed bed reactor model

The unsteady-state mass balance equations for species j in the dynamic and static liquid phases are similar to those presented by Lirachi et al. [9] for the co-current gas-liquid trickle-bed and packed-bubble column using the following assumptions:
1. The species accumulation, advection and axial dispersion are considered for the dynamic liquid phase.
2. Only the species accumulation is considered for the static liquid phase.
3. Mass transfer is considered across the dynamic-static liquid interface.
4. Contacting and mass transfer between catalyst and dynamic liquid is considered.
5. Contacting and mass transfer between catalyst and static liquid is considered.
6. Partial wetting and different efficiencies for static and dynamic liquid is considered.

The above assumptions lead to following mass balance equation for each species j for the dynamic and static liquid phases [9]:

$$\varepsilon_l^{d} \frac{\partial C_{jl}^{d}}{\partial t} + v_l \frac{\partial C_{jl}^{d}}{\partial z} = D_l \varepsilon_l^{d} \frac{\partial^2 C_{jl}^{d}}{\partial z^2} - (ka)_{ll}\left(C_{jl}^{d} - C_{jl}^{s}\right) - \eta_d k_{jls}^{d} a_s \left(C_{jl}^{d} - C_{jl}^{*}\right) \tag{9}$$

$$\varepsilon_l^{s} \frac{\partial C_{jl}^{s}}{\partial t} = (ka)_{ll}\left(C_{jl}^{d} - C_{jl}^{s}\right) - \eta_s k_{jls}^{s} a_s \left(C_{jl}^{s} - C_{jl}^{*}\right) \tag{10}$$

The Initial and boundary conditions for the above equations are:

$$t = 0 \rightarrow C_{jl}^{d} = C_{jl}^{s} = C_{jl}^{0} \tag{11}$$

$$z = 0 \rightarrow v_l C_{jl}^{0} = v_l C_{jl}^{d}\Big|_{z=0^+} - D_l \varepsilon_l^{d} \frac{\partial C_{jl}^{d}}{\partial z} \tag{12}$$

$$z = H \rightarrow \frac{\partial C_{jl}^{d}}{\partial z} = 0 \tag{13}$$

III. Reactor Operating Conditions for Simulation

The characteristics of the porous MnO_2/CeO_2 catalyst particles, the design and geometric parameters of the three-phase reactors and the operating conditions (base case) used in this investigation are presented in Table 1. Physical properties of water were used for the liquid phase. Under the mild pressure and temperature conditions employed in the simulations (0.5MPa and 80ºC), vapor and liquid phases were assumed to be ideal and Raoult's and Henry's laws were assumed valid for water and oxygen, respectively.

TABLE I
REACTOR DIMENSIONS AND OPERATING CONDITIONS USED IN THE SIMULATIONS

Temperature (ºC)	80
Total pressure (MPa)	0.5
Reactor diameter (m)	0.051
Bed height (m)	2
Catalyst particle size (mm)	3
Density of catalyst particle (kg/m³)	1760
Bed porosity (%)	36
Superficial liquid velocity (m/s)	0.0015
Superficial gas velocity (m/s)	0.028
Phenol feed concentration (mol/l)	0.001-0.03

IV. Numerical Solution

The set of partial differential equations (PDE) for the reactor models involve time and spatial partial derivatives for each species within the pellets and along the reactor. Solutions to these equations require a numerical algorithm and a priori estimates for a number of hydrodynamic, mass transfer, and kinetic parameters. For trickle beds, CWAO is usually carried out in the trickle flow regime under partial or full wetting conditions of pellets. Under similar operating conditions, however, the packed-bubble columns operate in the bubble flow regime with fully wetted pellets. The external liquid holdup, ε_l, can be estimated by the extended Holub model [13] for trickle beds, and by the neural network correlation of Bensetiti et al. [14] for packed-bubble columns. The static liquid holdup, ε_l^s, can be estimated from the Sáez and Carbonell correlation [15]. Accordingly, the dynamic liquid holdup, ε_l^d, is obtained by subtracting the static holdup from the external holdup. In trickle-bed operation, the catalyst wetting efficiency, η_e, is obtained by solving the phenomenological model of Iliuta et al. [16]. The static, η_s, and dynamic, η_d, components of wetting efficiency are obtained from an approximation suggested by Rajashekharam et al. [17]. The liquid-phase axial dispersion coefficients, D_l, and the mass transfer coefficients between dynamic and static liquids, $(Ka)_{ll}$, were taken from Reference [18] for trickle beds and from Reference [19] for packed-bubble columns. The (dynamic) liquid–solid mass transfer coefficient, k_{jls}^d, was estimated as an average from two literature correlations for trickle beds [20, 21] and packed-bubble columns [22-24]. The (static) liquid–solid mass transfer coefficient, k_{jls}^s, was estimated using Reference [25]. The effective diffusion coefficients, D_j^{eff}, were evaluated assuming a tortuosity factor of 3. The kinetic parameters were taken from Reference [10].

Different numerical algorithms can be employed for the solution of the set of PDEs outlined above. Larachie et al. [9] used the method of orthogonal collocation for discretization in the spatial dimension. We used an implicit finite difference scheme using 3-point central difference in the spatial dimension. The descritization was performed using 15 equal segments in the radial position within the pellet, 20 equal segments along the bed height, and a time step of 0.5 seconds. At each time step, the resulting set of non-linear algebraic equations was solved by the iterative Gauss-Seidel method with relaxation. Solution at the previous time step was used as the initial guess for the iterative procedure. A computer program using MATLAB was developed to perform the above algorithm for numerical solutions.

V. Results and Discussion

Solution of the equations outlined above would give the concentration profiles of species *j* within the catalyst pellet as well as their concentration in the static and dynamic liquid phases along the bed height with time. Phenol concentration in the dynamic liquid at the reactor exit was used to determine the exit conversion of phenol. The concentration profiles of phenol in the dynamic and static liquid versus bed height are presented in Figures 2 and 3, respectively, for the base case simulation for both the trickle-bed reactor (TBR) and packed-bubble column (PBC) at t = 5 hours.

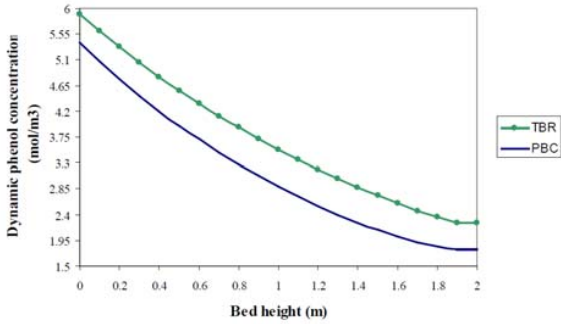

Fig. 2 Concentration of phenol in dynamic liquid phase vs. bed height fixed bed reactors $\left(C_{Al}^0 = 6\ mol/m^3, t = 5h\right)$

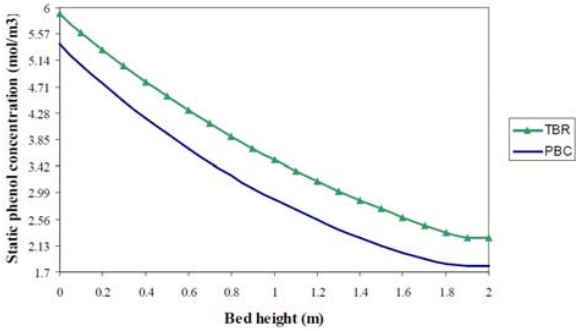

Fig. 3 Concentration of phenol in static liquid phase vs. bed height fixed bed reactors $\left(C_{Al}^0 = 6\ mol/m^3, t = 5h\right)$

The phenol conversion was about 62.3% for TBR and about 70% for PBC. The difference in the performance of the two reactors was due to the wetting efficiencies employed in the models. While full external wetting of the pellets was used for the PBC, the wetting efficiency used for TBR was 80%. The enhanced phenol conversion in PBC compared with TBR due to higher wetting efficiencies was observed regardless of feed phenol concentration. Phenol concentration profile in the static liquid along the bed followed the same trend as phenol

concentration in the dynamic liquid with concentration in the static liquid being slightly higher. The concentration profiles within the catalyst pellet are presented in Figure 4 at the half way point along the bed height at t=5 hours indicating that the reaction is highly diffusion limited and suggesting that the loss in catalyst activity would occur from the outside towards the pellet center in a progressive shell manner.

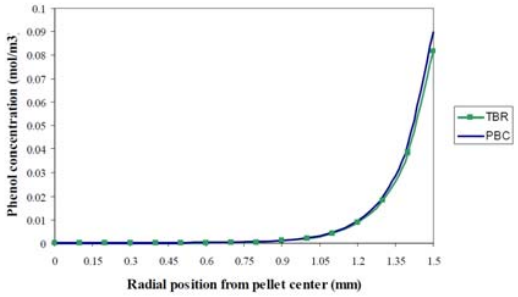

Fig. 4 Concentration of phenol inside catalyst pellets at mid-height of the reactor, Fixed bed reactors $\left(C_{Al}^{0} = 6\,mol/m^3, t = 5h\right)$

The effects of major operating parameters including superficial liquid velocity, size of catalyst pellets, and reaction temperature on the reactor performance was investigated by varying one parameter while keeping the rest the same as the base case simulation. Effects of different parameters are only presented for TBR since qualitative trends were similar for both TBR and PBC with only higher overall phenol conversions for the PBC.

Figure 5 illustrates the effect of liquid superficial velocity on phenol conversion at t =5 hours. As was expected, phenol conversion decreased with increasing liquid superficial velocity (lower liquid residence time). Figure 6 illustrates the effect of liquid superficial velocity on the local deactivation function within the catalyst pellet at the mid-height of the bed at t = 5 hours. With increasing liquid superficial velocity, the phenol concentration increased in both the dynamic liquid as well as in the interior of the catalyst thus enhancing the deactivation of the catalyst.

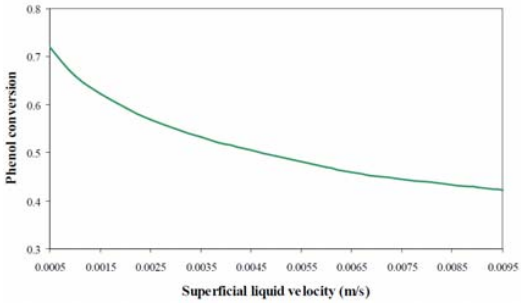

Fig. 5 Conversion of phenol vs. superficial liquid velocity, Trickle bed reactors $\left(C_{Al}^{0} = 6\,mol/m^3, t = 5h\right)$

Figure 7 illustrates the effect of catalyst pellet diameter on the conversion of phenol. With increasing pellet size, the external surface area of catalyst pellets per unit reactor volume was decreased thus causing a decrease in the overall mass transfer of phenol into the interior of the catalyst and consequently resulting in lower phenol conversions. Deactivation is also enhanced for larger catalyst particles due to the higher concentration of phenol.

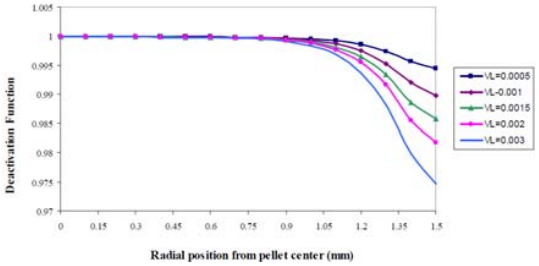

Fig. 6 Deactivation function inside catalyst pellets for different liquid superficial velocities at mid-height of the reactor, Trickle bed reactors $\left(C_{Al}^{0} = 6\,mol/m^3, t = 5h\right)$

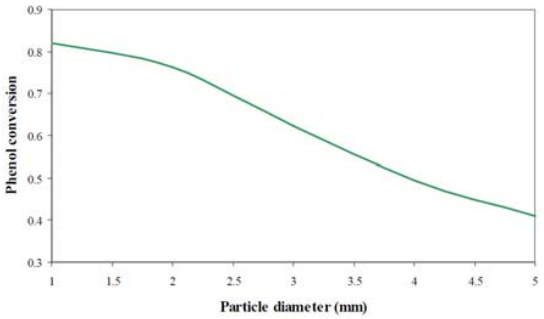

Fig. 7 Effect of particle diameter on phenol conversion, Trickle bed reactors $\left(C_{Al}^{0} = 6\,mol/m^3, t = 5h\right)$

Reaction temperature had a significant effect on the reactor performance. Many of the parameters used in the models including the kinetic constants for both the reaction rates and deactivation rate, as well as the mass transfer coefficients and hydrodynamic parameters including wetting efficiencies, liquid holdups, and axial dispersion coefficient are either directly or indirectly affected by temperature. Figure 8 illustrates the concentration profile of phenol in dynamic liquid along the bed height at t=5 hours for different temperatures indicating an increase in conversion with increasing reaction temperature. Catalyst deactivation is also enhanced with increasing temperature.

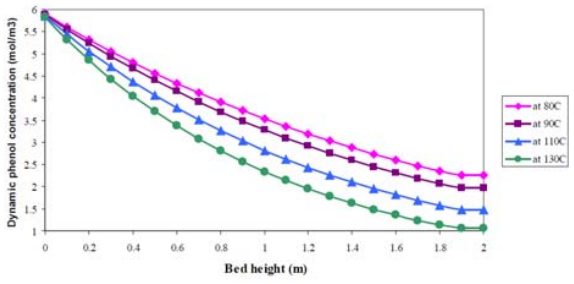

Fig. 8 Effect of temperature on concentration of phenol in dynamic liquid phase, Trickle bed reactors $\left(C_{Al}^{0} = 6\,mol/m^3, t = 5h\right)$

Figure 9 illustrates the effect of temperature on the local deactivation function within the catalyst pellet at the mid-height of the bed at t = 5 hours. The loss in catalyst activity is enhanced at higher reaction temperatures. Figure 10 also illustrates that with time on stream, the loss in catalyst activity is more severe for higher reaction temperatures. These observations point to an "optimum" reaction temperature as higher temperatures result in both higher initial activity and at the same time, higher rate of activity loss.

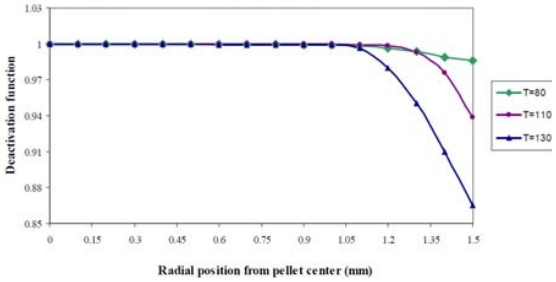

Fig. 9 Effect of temperature on the local deactivation function inside catalyst pellet, Trickle bed reactors $\left(C_{Al}^{0} = 6\ mol/m^3, t = 5h\right)$

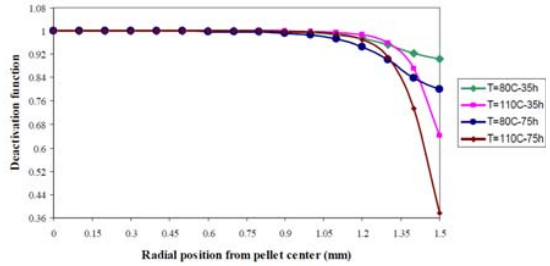

Fig. 10 Effect of temperature on the local deactivation function inside catalyst pellet at the mid height of the bed for different reaction times Trickle bed reactors $\left(C_{Al}^{0} = 6\ mol/m^3\right)$

Figure 11 illustrates the activity loss inside the catalyst pellet at the normalized radial position of r/r_p=0.934 with the bed height and Figure 12 shows the variations in the deactivation function within the catalyst pellet at the mid-height of the bed for the base case simulation for reaction times up to 200 hours. Allowing for minor differences in parameter values used for the model in the current investigation and those employed by Larichi et al. [9], and the difference in the numerical procedures employed in the two studies, the agreement between predictions of the two studies are satisfactory.

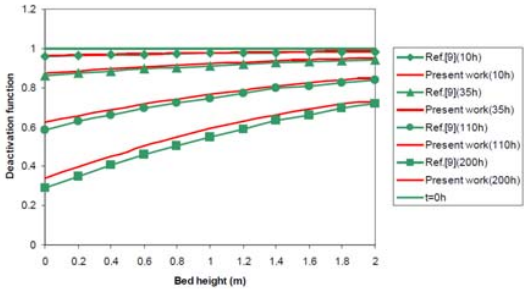

Fig. 11 Comparison of local deactivation function at dimensionless radial position of r/r_p=0.934 vs. bed height for reaction times up to 200 hours, Trickle bed reactors $\left(C_{Al}^{0} = 6\ mol/m^3\right)$

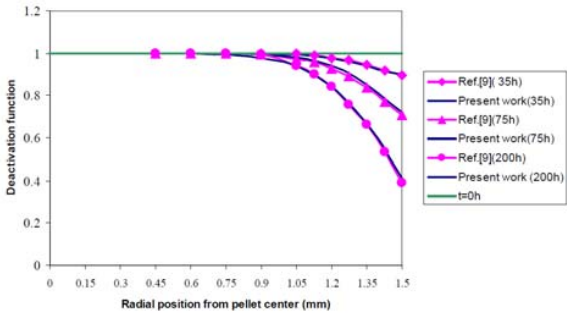

Fig. 12 Comparison of the local deactivation function inside catalyst pellet at mid-height of the reactor for reaction times up to 200 hours, Trickle bed reactors $\left(C_{Al}^{0} = 6\ mol/m^3\right)$

VI. Conclusions

A transient reactor model was employed for simulation of wet air catalytic oxidation of phenol. A comparative numerical analysis was performed for trickle-bed and packed-bubble column reactors. The modeling involved material balances both for the catalyst particle as well as for different fluid phases. Catalyst deactivation was also considered in a transient reactor model to investigate the effects of various parameters including reaction temperature, liquid superficial velocity, and catalyst pellet size on catalyst deactivation. The simulation results indicated that packed-bubble columns were slightly superior in performance than trickle beds due to higher wetting efficiencies. It was also found that reaction temperature was the most effective parameter in catalyst deactivation. Higher reaction temperatures resulted in both higher reaction rates as well as higher rate of deactivation suggesting that operation at an optimum temperature might be considered.

References

[1] V. S. Mishra, V. V. Mahajani, J. B. Joshi, "Wet air oxidation," *Ind. Eng. Chem. Res.*, vol. 34, pp. 2–48, 1995.
[2] S. K. Bhargava, J. Tardio, J. Prasad, K. Foger, D. B. Akolekar, S. C. Grocott, "Wet Oxidation and Catalytic Wet Oxidation," *Ind. Eng. Chem. Res.*, vol. 45, pp. 1221-1258, 2006.
[3] F. Luck, "A review of industrial catalytic wet air oxidation processes," *Catal. Today*, Vol. 27, pp. 195-202, 1996.
[4] S. Imamura, "Catalytic and nom-catalytic wet oxidation," *Ind. Eng. Chem. Res.*, vol. 38, pp.1743-1753, 1999.

[5] Y. I. Matatov-Meytal, M. Sheintuch, "Catalytic Abatement of Water Pollutants," *Ind. Eng. Chem. Res.,* vol. 37, pp. 309-326, 1998.
[6] P. L. Mills, R. V. Chaudhari, "Reaction engineering of emerging oxidation processes," *Catal. Today,* vol. 48, pp. 17-29, 1999.
[7] J. G. Rodrigo, M. Lopes, R. Quinta-Ferreira, "Trickle-bed CFD studies in the catalytic wet oxidation of phenolic acids," *Chem. Eng. Sci.,* vol. 62, pp. 7045–7052, 2007.
[8] A. Singh, K. K. Pant, K. D. P. Nigam, "Catalytic wet oxidation of phenol in a trickle-bed reactor" ,*Chem. Eng. J*., vol. 103**,** pp. 51–57, 2004.
[9] F. Larachi, I. Iliuta, K. Belkacemi, "Catalytic wet air oxidation with a deactivating catalyst analysis of fixed and sparged three-phase reactors," *Catal. Today*, vol. 64**,** pp. 309–320, 2001.
[10] S. Hamoudi, K. Belkacemi, F. Larachi, "Catalytic Oxidation of Aqueous Phenolic Solutions: Catalyst Deactivation and Kinetic," *Chem .Eng. Sci*., vol. 54, pp. 3569-3576, 1999.
[11] S. Hamoudi, F. Larachi, A. Adnot, A. Sayari, "Characterization of Spent MnO_2/CeO_2 Wet Oxidation Catalyst by TPO–MS, XPS and S-SIMS," *J. Catal.*, vol. 185, pp. 333-344, 1999.
[12] A. Pintar, J. Levec, "Catalytic oxidation of organics in aqueous solutions: I. Kinetics of phenol oxidation," *J. Catal.*, vol. 135, pp. 345-357, 1992.
[13] I. Iliuta, F. Larachi, B. P. A. Grandjean, "Pressure Drop and Liquid Holdup in Trickle Flow Reactors: Improved Ergun Constants and Slip Correlations for the Slit Model," *Ind. Eng. Chem. Res*., vol. 37, pp. 4542-4550, 1998.
[14] Z. Bensetiti, F. Larachi, B. P. A. Grandjean, G. Wild, "Liquid saturation in cocurrent upflow fixed-bed reactors: a state-of-the-art correlation", *Chem. Eng. Sci.*, vol. 52, pp. 4239-4247, 1997.
[15] A. E. Saez, R. G. Carbonell, "Hydrodynamic Parameters for Gas-Liquid Cocurrent Flow in Packed Beds," *AIChE J*., vol. 31, pp. 52-62, 1985.
[16] I. Iliuta, F. Larachi, B. P. A. Grandjean, "Catalyst Wetting in Trickle-Flow Reactors, A Phenomenological Model," *Chem. Eng. Res. Des*., vol. 77, pp. 759-763, 1999.
[17] M. V. Rajashekharam, R. Jaganathan, V. Chaudhari, "A trickle-bed reactor model for hydrogenation of 2, 4 dinitrotoluene: experimental verification," *Chem. Eng. Sci.*, vol. 53, pp. 787-805, 1998.
[18] I. Iliuta, F.C. Thyrion, O. Muntean, "Residence time distribution of the liquid in two-phase cocurrent downflow in packed beds: Air/newtonian and non-newtonian liquid systems," *Can. J. Chem. Eng.*, vol. 74, pp. 783-796, 1996.
[19] I. Iliuta, F.C. Thyrion, O. Muntean, M. Giot, "Residence time distribution of the liquid in gas-liquid cocurrent upflow fixed-bed reactors," *Chem. Eng. Sci*., vol. 51, pp. 4579-4593, 1996.
[20] S. Goto, J. M. Smith, "Trickle-bed reactor performance. Part I. Holdup and mass transfer effects," *AIChE J.*, vol. 21, pp. 706-713, 1975.
[21] C. N. Satterfield, M. W. Van Eek, G. S. Bliss, "Liquid-solid mass transfer in packed beds with downward concurrent gas-liquid flow," *AIChE J*., vol. 24, pp**.** 709-717, 1978.
[22] V. Speccia, G. Baldi, A. Gia netto, "Solid-Liquid Mass Transfer in Concurrent Two-Phase Flow through Packed Beds," *Ind. Eng. Chem. Proc. Des. Dev.,* vol. 17**,** pp. 362-367, 1978.
[23] S. Mochizuki, T. Matsui, "Liquid—solid mass transfer rate in liquid-gas upward cocurrent flow in packed beds," *Chem. Eng. Sci*., vol. 29, pp. 1328-1330, 1974.
[24] G. Delaunay, A. Storck, A. Laurent, J. Charpentier, "Electrochemical Study of Liquid-Solid Mass Transfer in Packed Beds with Upward Cocurrent Gas-Liquid Flow," *Ind. Eng. Chem. Proc. Des. Dev.*, vol. 19, pp. 514-521, 1980.
[25] I. Iliuta, F. Larachi, B. P. A. Grandjean, "Residence time, Mass transfer and Back-mixing of the Liquid in Trickle Flow Reactors Containing Porous Particles," *Chem. Eng. Sci.,* vol. 54, pp. 4099-4109, 1999.

NOMENCLATURE

a_s	external area of the particles per unit reactor volume (m^{-1})
C_j	concentration of lump *j* (kmol/m^3)
C_{jl}^0	*j*-component concentration in feed stream (kmol/m^3)
d_p	pellet diameter (mm)
D_j^{eff}	*j*-component effective diffusivity (m^2/s)
D_l	liquid axial dispersion coefficient (m^2/s)
H	bed height (m)
k, k'	lumped rate constants (mol/kg min)
K, K'	adsorption equilibrium constants (m^3/kmol)
k_{jls}	*j*-component liquid–solid mass transfer coefficient (m/s)
$(ka)_{li}$	mass transfer coefficient between dynamic and stagnant liquid zones (s^{-1})
r	radial position within catalyst particle (m)
r_j	reaction rate (mol/min kg catalyst)
r_p	radius of catalyst particle (m)
t	time (s)
v_l	liquid superficial velocity (m/s)
X	phenol conversion
Z	longitudinal coordinate (m)
	Greek symbols
α	deactivation function
ε_l	liquid holdup
ε_p	particle internal porosity
η_d	dynamic external wetting efficiency
η_e	external wetting efficiency
η_s	static external wetting efficiency,
ρ_s	catalyst particle density (kg/m3)
φ	fraction of dynamic liquid
	Subscripts
A	phenolic carbon, A lump
B	carbon of oxidation intermediates, B lump
C	carbon of fully mineralized products, C lump
d	dynamic
l	liquid
s	static
	Superscripts
d	dynamic
s	static
*	on catalyst surface
o	feed